Title

Outer retinal abnormalities associated with inner retinal pathology in nonglaucomatous and glaucomatous optic neuropathies

Journal

Eye, 25(3)

ISSN

0950-222X

Authors

Werner, JS
Keltner, JL
Zawadzki, RJ
et al.

Publication Date

2011-03-01

DOI

10.1038/eye.2010.218

Peer reviewed

Eye (2011) 25, 279–289

www.nature.com/eye

CAMBRIDGE OPHTHALMOLOGICAL SYMPOSIUM

Outer retinal abnormalities associated with inner retinal pathology in nonglaucomatous and glaucomatous optic neuropathies

JS Werner[1,2], JL Keltner[1,3], RJ Zawadzki[1] and SS Choi[1,4]

Abstract

Inner and outer retinal morphology were quantified *in vivo* for 6 nonglaucomatous and 10 glaucomatous optic neuropathy patients. Custom, ultrahigh-resolution imaging modalities were used to evaluate segmented retinal layer thickness in 3D volumes (Fourier-domain optical coherence tomography), cone photoreceptor density (adaptive optics fundus camera), and the length of inner and outer segments of cone photoreceptors (adaptive optics–optical coherence tomography). Quantitative comparisons were made with age-matched controls, or by comparing affected and nonaffected retinal areas defined by changes in visual fields. The integrity of outer retinal layers on optical coherence tomography B-scans and density of cone photoreceptors were correlated with visual field sensitivity at corresponding retinal locations following reductions in inner retinal thickness. The photoreceptor outer segments were shorter and exhibited greater variability in retinal areas associated with visual field losses compared with normal or less affected areas of the same patient's visual field. These results demonstrate that nonglaucomatous and glaucomatous optic neuropathies are associated with outer retinal changes following long-term inner retinal pathology.
Eye (2011) **25,** 279–289; doi:10.1038/eye.2010.218; published online 4 February 2011

Keywords: optic nerve diseases; cone photoreceptors; retinal imaging

Introduction

The optic neuropathies are a diverse group of diseases that have a wide range of origins, including heredity, trauma and compression, ischemia, metabolic or toxic disturbances, and unknown etiologies.[1] Nevertheless, the optic neuropathies have a common manifestation: damage to the retinal ganglion cells,[2–6] usually beginning with axonal degeneration or demyelination followed by retrograde degeneration to the cell body and anterograde degeneration to central projection sites. Clinical diagnosis is based on ophthalmoscopically visible abnormalities of the optic disk color and shape, with accompanying changes in the retinal vasculature and retinal nerve fiber layer. Quantification of nerve fiber layer integrity by optical coherence tomography (OCT)[7,8] or scanning laser polarimetry, and visual field changes[9,10] are often important in differential diagnosis of these disorders.

Additional visual symptoms in various types of optic neuropathy include loss of visual acuity, impaired contrast sensitivity,[11,12] and decreased color discrimination.[13,14] In acquired deficiencies of color, Köllner's rule[15] posits that red–green color defects are more often associated with optic nerve and central diseases, whereas tritan defects are more often associated with changes in the outer retina. Yet, patients with optic neuritis have mixed color vision changes[16] and patients with glaucoma often show yellow–blue changes.[17,18] This would suggest that outer retinal changes may accompany optic neuropathies, but an alternative explanation might be that there is selective loss in ganglion cells carrying

[1]Department of Ophthalmology and Vision Science, Davis Eye Center, University of California, Davis, CA, USA

[2]Department of Neurobiology, Physiology and Behavior, University of California, Davis, CA, USA

[3]Departments of Neurology and Neurological Surgery, University of California, Davis, CA, USA

[4]New England College of Optometry, Boston, MA, USA

Correspondence: JS Werner, Departments of Ophthalmology and Vision Science and Neurobiology, Physiology and Behavior, Davis Eye Center, University of California, 4860 Y Street, Suite 2400, Davis, CA 95817, USA
Tel: +1 916 734 6817;
Fax: +1 916 734 4543.
E-mail: jswerner@ucdavis.edu

Received: 3 November 2010
Accepted: 23 November 2010
Published online: 4 February 2011

Presented at the Cambridge Ophthalmological Symposium.

signals from the short-wave sensitive cones.[19] The electroretinogram a-wave and multifocal responses are dominated by photoreceptors and bipolar cell signals, and studies of optic neuropathy patients provide further evidence that outer retinal changes may sometimes,[20,21] but not invariably,[22,23] occur.

Anatomical changes would seemingly settle the issue as to whether there are upstream changes in optic neuropathies, but these results are also equivocal. Swelling and loss of photoreceptors have been reported in human and monkey model[24,25] in conjunction with retinal ganglion cell damage. This is not, however, supported by other studies[26,27] in which the outer retina of glaucoma patients was examined histologically.

Here, we review results obtained from our laboratory from carefully classified patients having nonglaucomatous or glaucomatous optic neuropathies. *In vivo* imaging was carried out with three research-grade high-resolution instruments[28–30] that permitted quantification of inner and outer retinal morphology and correlation with visual fields. The results demonstrate both inner and outer retinal changes in both nonglaucomatous and glaucomatous optic neuropathies when there were stable and long-standing losses in visual fields.

Subjects and methods

Subjects

Six patients, age 34–67 years, with nonglaucomatous optic neuropathy were tested: three with multiple sclerosis (MS), one with bilateral nonarteritic anterior ischemic optic neuropathy (NAION), one with bilateral optic nerve head drusen and NAION, and one with idiopathic intracranial hypertension (IIH; pseudotumor cerebri). Ten patients with glaucoma were also included: one with pigmentary dispersion glaucoma, seven with primary open-angle glaucoma, and two with normal tension glaucoma. Seven normal subjects (21–58 years old) were recruited for direct comparisons of various aspects of retinal morphology.

All participants were screened with comprehensive clinical examinations. Patients were additionally examined by a neuro-ophthalmologist and/or glaucoma specialist. Screening included direct and indirect ophthalmoscopy, visual field analysis, and Stratus (Zeiss Meditec, Dublin, CA, USA) OCT imaging. All glaucoma patients had enlarged cup-to-disc ratios with thinning of neural rims. Most exhibited additional changes such as disk hemorrhages, peripapillary atrophy, focal notching, and visual field defects. Refractive error was an exlusionary criterion only if it exceeded ± 3D spherical and ± 3D cylinder.

Procedure

Written informed consent was obtained from each participant after explaining the procedures and before any experimental measurements. The Tenets of the Declaration of Helsinki were observed throughout, and the protocol was approved by the Institutional Review Board of the University of California, Davis, School of Medicine.

Three laboratory instruments were used for ultrahigh-resolution imaging. Each instrument included a calibrated fixation target so that images from the different modalities could be registered. Subject alignment was maintained by the use of a dental-impression bite-bar and forehead rest. Before image acquisition, eye drops were used to induce cycloplegia and pupil dilation.

In addition to vision science goals, our laboratory has engineering goals for improvement of image acquisition and post-processing. In achieving the latter objectives, some instruments were modified over the course of our studies. However, our instruments had sufficient resolution at all times for the imaging described in this paper. Here, we describe briefly recent versions of these instruments.

Fourier-domain optical coherence tomography

This instrument is a fiber-based Michelson interferometer permitting acquisition of cross-sectional retinal images (B-scans; 18° field of view) that can be registered to form volumes for layer segmentation.[31] An example from a normal 34-year-old observer is shown in Figure 1. Our instrument is similar to commercial Fourier-domain optical coherence tomography systems, but has higher theoretical axial resolution (3.6 μm) owing to a broader bandwidth light source, a superluminescent diode (Superlum, Carrigtwohill, Co. Cork, Ireland) with an 852 nm central wavelength and 79 nm FWHM. The beam power incident on the cornea is 450 μW. The theoretical lateral resolution is 10 μm. This system uses one of two line detectors: CCD (Atmel, San Jose, CA, USA) for standard speed acquisition (up to 24 frames/s with 1000 A-scans) and CMOS (Basler, Ahrensburg, Germany) for high-speed acquisition (up to 125 frames/s with 1000 A-scans). Other details are published elsewhere.[32]

Adaptive optics fundus camera (AO-FC)

This instrument is designed to provide *en face* images with high lateral resolution for imaging the cone photoreceptor mosaic. It does so by measuring the observer's wavefront aberrations and then correcting the higher-order aberrations in a closed-loop system.[33] Lower-order aberrations, sphere and cylinder, are corrected with trial lenses in the spectacle plane. Briefly, the pupil is imaged onto a Shack-Hartmann wavefront sensor with a 20×20 lenslet array across a 6 mm pupil.

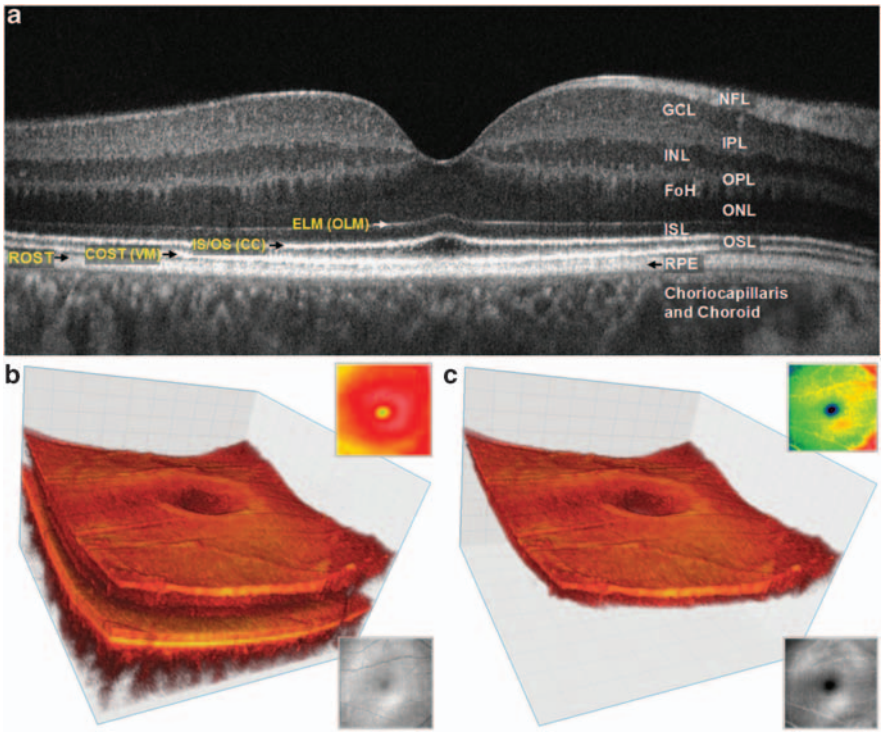

Figure 1 (a) Fourier-domain optical coherence tomography (FD-OCT) B-scan of the fovea from a normal 34-year-old volunteer acquired with our FD-OCT instrument scanning 5 mm laterally. Abbreviations: FoH, fibers of Henle; GCL, ganglion cell layer; INL, inner nuclear layer; IPL, inner plexiform layer; ISL, inner segment layer; NFL, nerve fiber layer; ONL, outer nuclear layer; OPL, outer plexiform layer; OSL, outer segment layer; RPE, retinal pigment epithelium, choriocapillaris and choroid. The outer limiting membrane (OLM; sometimes called external limiting membrane (ELM)), connecting cilia (CC; sometimes called inner/outer segment junction), Verhoeff's membrane (VM; sometimes called cone photoreceptor outer segment tips (COST)) and rod photoreceptor outer segment tips (ROST) may also be seen. ROST and RPE appear as one layer in the fovea but are visible as separate layers in the periphery. The fibers of Henle cannot be clearly distinguished from the ONL in this image. The inner limiting membrane and Bruch's membrane are not visible on this image, but have been confirmed using the same OCT system for imaging retinal dystrophies. (b) Volumetric reconstruction of central foveal region from 100 B-scans from the same observer in (a). Small insets show total retina thickness map (top right) and OCT fundus view (*en face* projection) for this data set (bottom right). (c) Volumetric reconstruction of segmented three-layer inner retinal complex extracted from volume (b). Small insets show three-layer complex thickness map (top right) and OCT fundus view (*en face* projection) for three-layer complex only (bottom right).

A superluminescent diode operating at 835 ± 20 nm is used to form a reference spot on the retina for wavefront sensing. High-order aberrations are corrected with a 68 mm, 109 actuator, continuous surface deformable mirror (DM; Litton ITEK, Lexington, MA, USA) that has an approximate mirror stroke of $\pm 2\,\mu$m. Direct slope control is used for the individual DM actuators. The wavefront is sampled at 20 Hz, yielding a closed-loop bandwidth of ~ 0.9 Hz and a gain of 30%. After minimizing wavefront error, an imaging source (300 W xenon lamp), shaped spectrally by an interference filter (550 or 650 ± 40 nm), is passed to the retina and back-reflected following the corrected path of the DM and is re-imaged onto a cooled CCD camera (VersArray XP; Princeton Instruments, Monmouth, NJ, USA). The exposure duration is 10 ms with 0.25 μJ of light delivered through a 2.4 mm diameter entrance pupil. The imaging camera is translated axially on a motorized stage to correct for the ocular longitudinal chromatic aberration between the wavefront sensor beacon at 835 nm and the visible wavelengths used for imaging. The resultant images have a field of view of 1° with 2.5 μm lateral resolution, sufficient to image cone photoreceptors outside the foveola. Custom software permits semi-automatic cone counting,[34] as illustrated in Figure 2. Cone densities were corrected for the presence of blood vessels in the image.

Adaptive optics-optical coherence tomography (AO-OCT)
The purpose of this instrument is to produce 3D isotropic ultrahigh-resolution retinal images. This is possible because axial and lateral resolution are largely independent in AO-OCT such that the major advantages of each modality can be realized.[35–37] One limitation in this approach is that when the bandwidth of the OCT imaging beam increases to achieve maximal axial

resolution, there may be a loss in lateral resolution due to the longitudinal chromatic aberration of the eye. This can be compensated to a large extent by use of a custom achromatizing lens, which we place in the sample arm.[37]

In our system, the light source used for both OCT and wavefront sensing is a superluminescent diode (Superlum BroadLighter, Superlum) having a central wavelength of 836 nm and bandwidth of 112 nm. The light level at the entrance pupil of the subject's eye does not exceed 400 μW. The AO arm of this system cascades two wavefront correctors, a large stroke 37-actuator bimorph DM (AOptix, Campbell, CA, USA), and a micro-electromechanical system (MEMS) 140-actuator DM (Boston Micromachines, Cambridge, MA, USA). The high-stroke DM permits imaging without trial lenses, which would otherwise cause a dispersion difference between the reference and sample arms. The two DMs are not operated simultaneously; rather, the optimized correction with the AOptix DM is fixed after the wavefront error is minimized, and then the MEMS DM is operated to improve aberration correction by operating in a closed loop at a rate of 16 Hz. By use of two DMs it is also possible to shift the focus so that maximal resolution occurs for layers of interest, as illustrated by Figure 3. With diffraction-limited correction, the resolution is $\sim$3.0 μm in all three directions over a field of view of $3^\circ \times 3^\circ$.

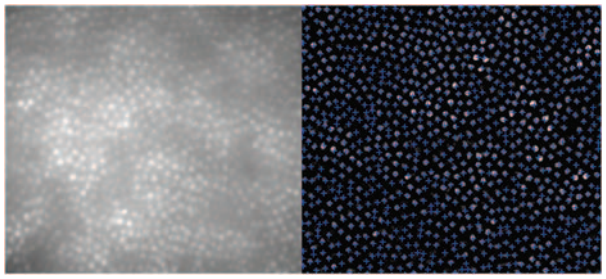

Figure 2 Left: Cone photoreceptor mosaic at 4° temporal retina of a normal 22-year-old volunteer acquired with our AO-FC (imaging wavelength = 550 nm). Right: Results of automatic cone-counting algorithm for image on the left, with all cones accurately identified (25 164 cones/mm^2).

Results

Maps of inner retina in optic neuropathies

Although the image presented in Figure 1 from a normal observer shows a well-delineated retinal nerve fiber layer that is easily segmented from the 3D volume, it is often not as well defined in individuals with optic

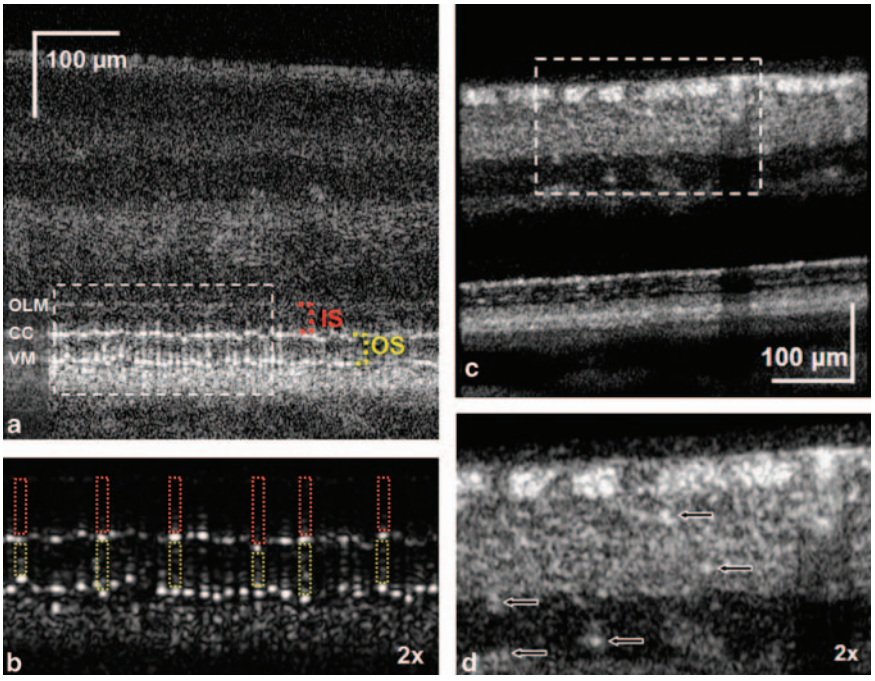

Figure 3 (a) Ultrahigh-resolution AO-OCT B-scan (500 A-scans corresponding to 0.5 mm) acquired at 4.5° nasal retina of the same volunteer as in Figure 1, in which the AO-system focus was set on the outer retina. Dashed rectangle corresponds to the magnified region shown in (b). (b) Two-fold enlargement and linear intensity scale image of the photoreceptor layer from (a). Dashed red rectangles show examples of cone photoreceptor inner segments (IS). Dashed yellow rectangles show examples of cone photoreceptor outer segments (OS). (c) An average of 10 AO-UHR-OCT frames acquired at 9° superior 4.5° nasal eccentricity of a healthy 55-year-old volunteer (500 A-scans over line of 0.5 mm). Dashed rectangle corresponds to the magnified region shown in (d). (d) Two-fold enlargement of the rectangular area of inner retina in (c). Arrows indicate location of micro-capillaries in the inner retina.

neuropathies. In those cases, segmentation is more reliable if a combined three-layer inner retinal complex (retinal nerve fiber layer, ganglion cell layer, and inner plexiform layer) is segmented. From the extracted retinal layers, an *en face* thickness map may be constructed.

As expected from previous work,[38,39] the thickness of the inner retinal complex is reduced in individuals who have a loss in visual field sensitivity. For example, Figure 4 shows a normal 35-year-old subject and an MS patient, age 43 years, having a borderline normal

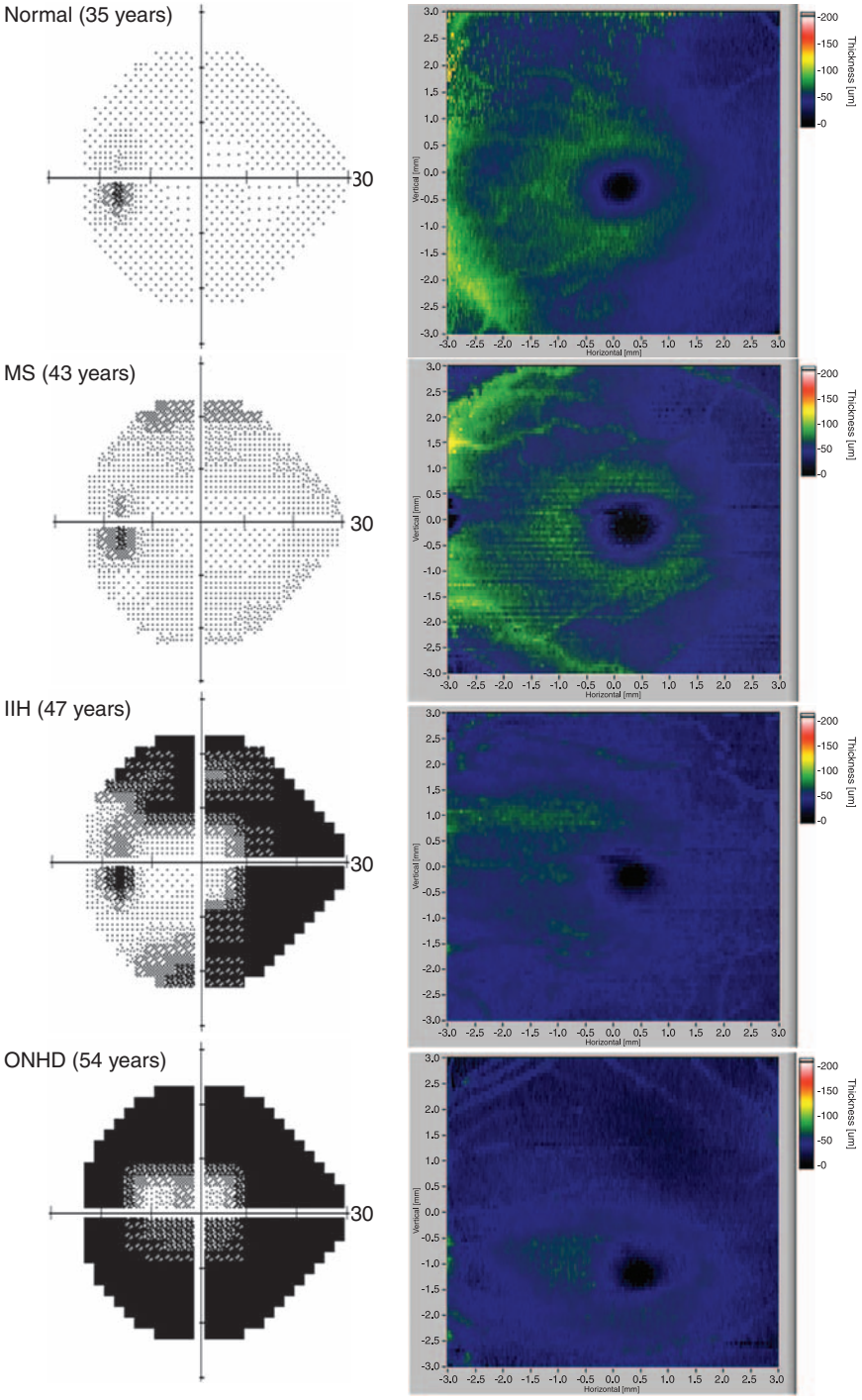

Figure 4 Left column shows visual field maps (HVF 24-2); right column shows corresponding two-dimensional thickness maps of the three-layer inner retinal complex (NFL + GCL + IPL) around the macula. All figures show left eye. Rows from top down: normal retina, multiple sclerosis (MS), idiopathic intracranial hypertension (IIH), and optic nerve head drusen (ONHD) with NAION.

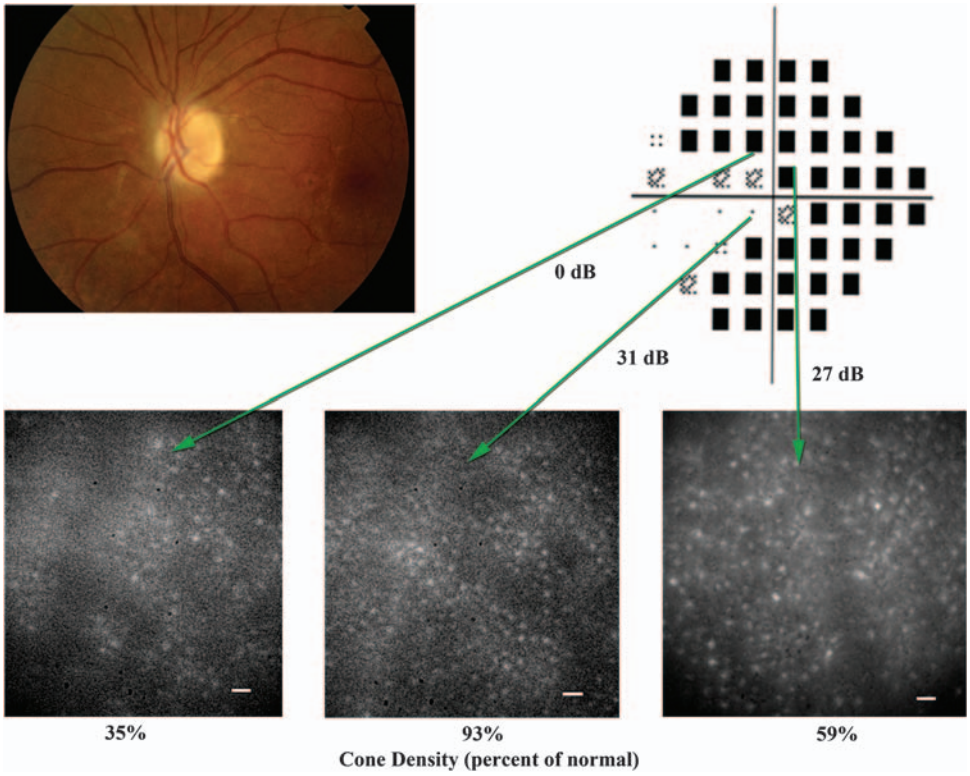

Figure 5 Optic disk photo (upper left) of left eye of patient with idiopathic intracranial hypertension showing 3+ optic nerve pallor and normal vasculature. Total deviation map (upper right) is based on SITA Standard 24-2 HVF, size III stimulus. The mean deviation was −21.84 with 37 dB foveal threshold. Visual field sensitivities (dB) for the imaged areas are shown. Lower row shows *en face* images of cone mosaics for three retinal regions of varying sensitivity. Scale bar = 10 μm.

field with some scattered missed spots in the periphery. Their inner retinal thickness maps were similar, with the thickness ranging between 50 and 110 μm. In contrast, optic neuropathy patients with stable visual field losses showed a reduction in inner retinal thickness. Figure 4 (lower two panels) shows visual field and inner retinal thickness maps for patients with IIH (age 47) and optic nerve head drusen with NAION (age 54). Visual fields were measured with the HVF SITA 24-2 algorithm, size III stimulus. Both the IIH and NAION patients showed marked constriction of visual fields with macular sparing. In both cases, the thickness of the inner retinal complex ranged from ~0–50 μm to 75 μm for small patches in the IIH patient. The thickness distribution was correlated with visual fields, showing reduced thickness at the locations where visual sensitivity is reduced, and increased thickness over areas with higher visual sensitivity.

All nonglaucomatous and glaucomatous optic neuropathy patients showed reductions in the thickness of the three-layer complex, provided they had long-term losses in visual field sensitivity. To examine whether there may also be changes in outer retinae of these patients, visual field maps were used to guide the choice of locations for ultrahigh-resolution imaging.

Outer retinal changes in nonglaucomatous optic neuropathies

Outer retinal morphology was examined by Fourier-domain optical coherence tomography and AO-OCT to determine the integrity of the three layers anterior to the RPE, the external limiting membrane (ELM), connecting cilia (between inner (IS) and outer segments (OS)), and Verhoeff's membrane, where the cone outer segment tips are enveloped by microvilli from the RPE. In addition, the AO-FC was used to acquire *en face* images of cone photoreceptor mosaics. Population statistics to evaluate losses in cone density are limited; however, outside the fovea, cone counts that we[34] and others[40] obtain from normal retinae *in vivo* agree well with histological counts[41] reported for normal retina. Therefore, we use the latter as a reference and specify densities obtained from patient AO-FC images in terms of percentages of what is expected from normal

histology. Here, we present results from two patients having nonglaucomatous optic neuropathy.

Photoreceptor mosaics from the left eye of a 47-year-old female with IIH, or pseudotumor cerebri, are shown in Figure 5. This patient had bilateral optic nerve pallor as seen in her fundus photos; the thickness map of her inner retina is presented in Figure 4 along with the gray scale visual field map from the SITA Standard 24-2 HVF. In this figure, we see the total deviation map, which was predictive of regions of corresponding reduction in cone density, which varied left to right in the figure from 8028 per mm^2 at 2° nasal, 7° inferior, 16 169 per mm^2 at 4° nasal, 4° inferior retina, to 10 306 at 4° temporal, 4° inferior. These cone densities are 35, 93, and 59%, respectively, of normal values. Thus, in addition to expected inner retinal pathology, there is also outer retinal abnormality in this patient.

A second nonglaucomatous optic neuropathy patient was a 54-year-old male with optic nerve drusen. He was a smoker who, at age 19, woke up with painless vision loss following dehydration from hiking at high altitude. He sustained severe constriction of visual fields, but preserved central vision (VA = 20/15). Figure 4 (bottom) shows his severe loss of visual field and inner retina. He had been extensively tested for many years and was, therefore, described in a separate case study.[29] It is presumed that he had NAION, but this was not verifiable given the long lapse between his acute vision loss and first examination.

Figure 6 presents his total deviation map from a 10-2 visual field and *en face* images of his cone mosaic at two retinal locations, corresponding to regions of normal and abnormal visual field sensitivity. In the normal region of inferior visual field (corresponding to 2° superior retina), his cone density was 21 885 cones/mm^2 which is 89% of the cone density expected. In contrast, in an area of severe vision loss and inner retinal changes (8° temporal, 8° inferior retina), he has only 5594 cones/mm^2, which is 57% of what is expected from normal retina. The other eye of this patient showed similar cone densities for areas of the visual field that had comparable visual field sensitivity losses.

As can be seen in Figure 1, three well-defined contours anterior to the RPE may be identified in normal outer

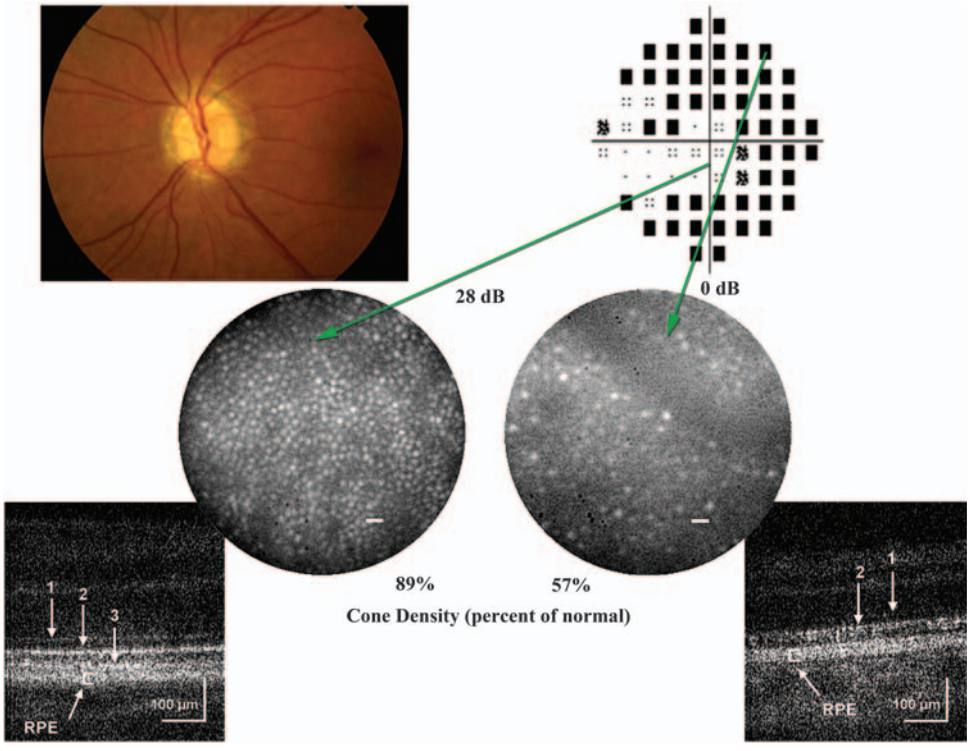

Figure 6 Optic disc photo (upper left) of left eye with 4+ optic nerve drusen. Upper right shows total deviation map from HVF 10-2 measured with Size III test target. The mean deviation was −15.92 dB with normal foveal threshold of 33 dB. Visual field sensitivities (dB) for the imaged areas are shown. Arrows show corresponding *en face* images of the cone mosaic. Scale bar = 10 μm. Next to each is a corresponding AO-OCT B-scan with focus on the outer retina. Numbers 1, 2, and 3 refer to outer limiting membrane, connecting cilia (or inner/outer segment junction) and Verhoeff's membrane (cone photoreceptor outer segment tips), respectively. Note that the left B-scan is normal with three visible outer retinal layers and the right is abnormal with only two visible outer retinal layers. Scale bar = 100 μm.

retina. The top layer represents the ELM, the second layer is at the junctions between the IS and OS of cone photoreceptors (IS/OS), and the third layer is Verhoeff's membrane. With AO-OCT, gaps in the layers are ascribable to gaps between adjacent cones (see Figure 3 left). Note that in our patient shown in Figure 6, the area with a more intact cone mosaic (2° superior retina) in AO-FC images, there are three distinct contours in the outer retina, whereas in the area with an abnormal cone mosaic (8° temporal, 8° inferior retina), Verhoeff's membrane is not visible. This observation is consistent with cone losses due to dystrophy of the outer segments.

Among the other nonglaucomatous optic neuropathy patients, there were three MS patients tested. It is noteworthy that one showed a normal cone mosaic, whereas another showed a more abnormal cone mosaic than expected from data of other optic neuropathy patients. The MS patient with a normal cone mosaic was a 34-year-old female with fluctuating visual field defects and mild optic disk pallor in both eyes. The AO-FC images showed normal cone densities in the four regions of retina tested. Eight months later, she had normal visual fields, consistent with the conclusion that upstream retinal changes occur only after sustained loss of visual fields. More severe visual field defects of a long-standing nature were documented for a 45-year-old female MS patient with bilateral optic atrophy combined with systemic lupus erythematosus and arthritis. This individual had cone densities that were only 3–27% of expected normal values in the right eye and 27–52% in the left eye. These cone losses were greater than those associated with comparable visual field losses in other patients. It is not clear why this occurred, but it may be related to her serious systemic, as well as neuro-ophthalmological, conditions. To further examine these losses in cone density, we considered that perhaps more cones were present but not visible because of changes in their directional sensitivity. This was tested by measuring the optical Stiles–Crawford effect,[42] in which the imaging light for the AO fundus camera was varied in 1 mm increments along the horizontal axis of the entrance pupil. If there is a systematic change in angular tuning of the photoreceptors that caused a change in cone visibility, it is expected that changing the entrance pupil would reveal them as normal retina, which is characterized by little disarray over the imaging apertures of our methods. For this MS patient, the Stiles–Crawford effect was examined over a patch

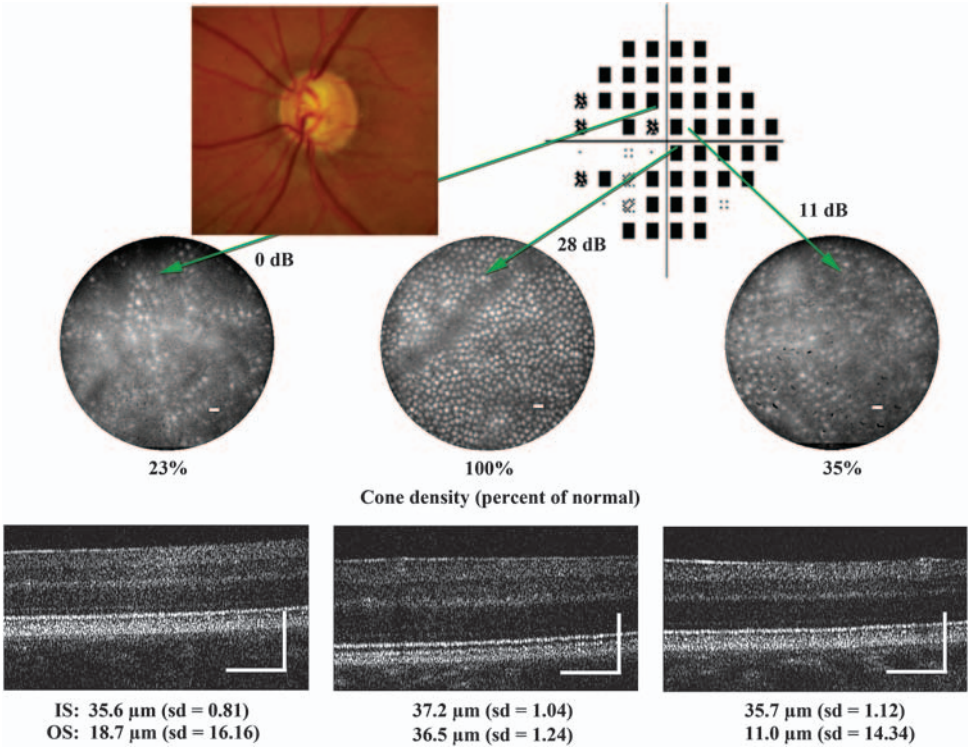

Figure 7 Upper left shows the left optic disc of a 25-year-old with pigmentary dispersion glaucoma. Upper right is the HVF 24-2 total deviation plot; mean deviation was −16.37 dB and the foveal threshold was 35 dB. Visual field sensitivities (dB) for the imaged areas are shown. *En face* images of the cone photoreceptors and corresponding AO-OCT B-scans at three retinal locations are shown. Mean length and standard deviation of inner (IS) and outer segments (OS) are shown for each retinal location.

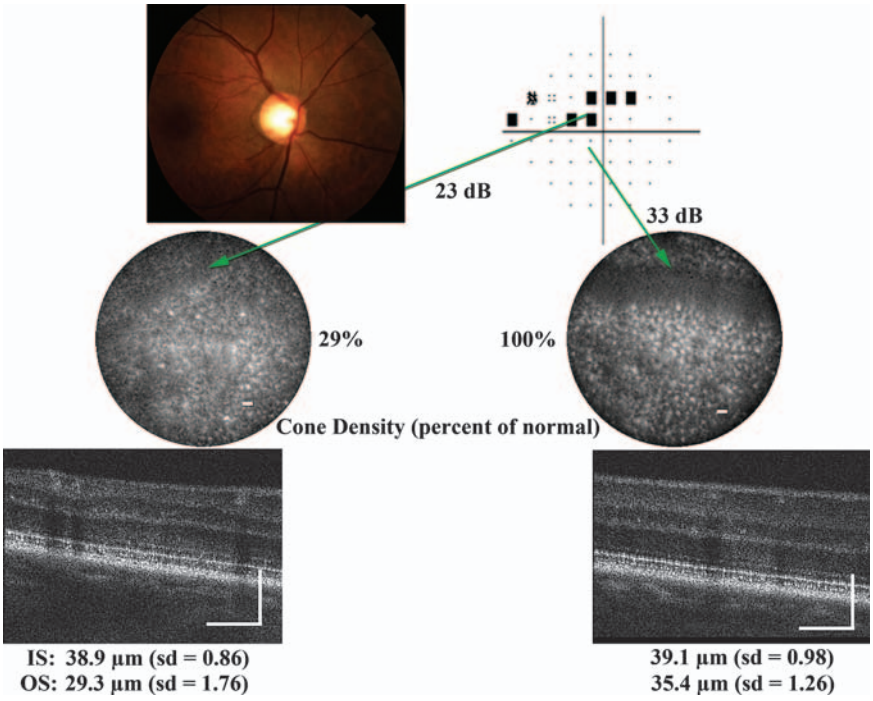

Figure 8 Optic disc photo and total deviation map from HVF 24-2 from the right eye of a 63-year-old patient with primary open-angle glaucoma. Mean deviation was −2.58 dB and the foveal threshold was 36 dB. Visual field sensitivities (dB) for the imaged areas are indicated. Arrows show the high-resolution retinal images from areas of higher and lower visual sensitivity. Mean length and standard deviation of inner (IS) and outer segments (OS) are shown for each retinal location.

of retina at 4° temporal, 4° superior in the right eye. With different entrance pupils, some cones were revealed that were not previously visible, while others that were previously visible were no longer visible. The net effect is that misidentification of cones due to possible disruptions of their waveguide properties would only affect cone counts by a few percent in this patient. Combining all the cones at the various entrance pupil positions still results in cone density substantially below that expected in a healthy eye.

Outer retinal changes in glaucomatous optic neuropathies

The analysis of images with glaucomatous optic neuropathies was similar to those described above, but in addition, AO-OCT images were used to measure the length of IS and OS of cone photoreceptors. IS length was defined as the distance between the ELM and the IS/OS junction of a single cell ('dot') positioned directly underneath the ELM. OS length refers to the distance between two 'dots' that can be vertically paired at the junctions of IS/OS and OS/RPE representing a single cone photoreceptor. In most cases, areas of normal and abnormal visual sensitivity were used to select locations that were equidistant from the foveola.

Figure 7 shows the enlarged cup and notch of the optic disk in the fundus image of a 25-year-old male with pigmentary dispersion glaucoma. His visual field is characterized by a superior arcuate defect and an inferior partial arcuate defect. Note that one of the regions of visual field chosen is depicted as abnormal in the total deviation plot, but is relatively normal (28 dB) compared with the other areas. Three areas of retina corresponding to different visual field sensitivities are shown. Cone densities from left to right were 5890, 24 400, and 5556 cones/mm^2, representing 23, 100, and 35%, respectively, of the expected normal values for these retinal loci. The AO-OCT images show that only the area with 100% of normal cone density is associated with three discrete outer retinal layers. As shown by the values listed below the AO-OCT B-scans, the cone IS lengths were similar at all retinal locations. However, there was a significant difference in OS lengths among the three areas, with the areas of reduced cone density having lower mean lengths and higher variability.

The results for the right eye of a primary open-angle glaucoma patient (age 63 years) are presented in Figure 8. The HVF 24-2 shows a mild superior arcuate defect. *En face* images from areas of high- and low-visual

sensitivity show cone densities varying from 29% (4.5° temporal, 4.5° inferior retina) to 100% (4.5° temporal, 4.5° superior retina) of expected cone density. The three layers in the outer retina are more clearly demarcated above the RPE in the area of higher visual sensitivity. Whereas the IS lengths do not vary for the two locations, the OS are shorter and more variable in the retinal area with lower sensitivity and lower cone density.

All glaucoma patients tested showed a similar pattern of results to those shown in Figures 7 and 8. Areas of reduced visual field sensitivity were not different from normal areas in their IS lengths, whereas the OS lengths were shorter and more variable in retinal areas associated with sensitivity loss. These results support the conclusion that the reduced cone densities revealed in *en face* images are due to reduction in the OS lengths. These same areas show a disruption in visibility of Verhoeff's membrane.

Conclusions

Despite the diverse etiologies of optic neuropathies, upstream losses in the outer retina have been identified in all cases manifesting *long-term* visual field loss and *following* thinning of the three-layer inner retinal complex. Structural changes in outer retina are thought to lag visual field changes and losses in inner retina so that the quantitative relations between inner and outer retinal changes are likely to depend on the state of disease progression, and this may also vary with the particular type of optic neuropathy. Nevertheless, in areas of sustained visual field abnormality, we consistently observed that cone photoreceptors were less reflective, resulting in dark regions in the *en face* images, and there was disruption of outer retinal layers in corresponding areas revealed by high-resolution OCT and AO-OCT images. In cases of transient visual field impairment and normal inner retina, there were no detectable upstream abnormalities in outer retina. The cones were densely packed and the integrity of the outer retina was implied by intact Verhoeff's membrane.

The data presented here are buttressed by related studies, which together[24,25,43] demonstrate that outer retina is vulnerable in nonglaucomatous and glaucomatous optic neuropathies. It would be surprising if prolonged visual field loss were accompanied by changes restricted to the nerve fiber layer and ganglion cells without affecting other retinal layers including photoreceptors. All of the patients we tested exhibited a strong association between structural changes in cone photoreceptors and loss of visual sensitivity as well as thinning of the three-layer inner retinal complex. It will be important to understand the remodeling that takes place in all parts of retina associated with optic neuropathies to effect better monitoring, interventions and therapies for these severely blinding diseases.

Conflict of interest

The authors declare no conflict of interest.

Acknowledgements

Funded by the National Eye Institute (EY 014743), National Institute on Aging (AG 04058) and Research to Prevent Blindness.

References

1 Miller NR, Newman NJ. *Walsh & Hoyt's Clinical Neuro-Ophthalmology*, 6th ed. Lippincott, Williams & Wilkins: Philadelphia, 2005.
2 Waxman SG. Membranes, myelin and the pathophysiology of multiple sclerosis. *N Engl J Med* 1982; **306**: 1529–1533.
3 Katz BJ, Pomeranz HD. Visual field defects and retinal nerve fiber layer defects in eyes with buried optic nerve drusen. *Am J Ophthalmol* 2006; **141**: 248–253.
4 Bianchi-Marzoli S, Rizzo III JF, Brancato R, Lessell S. Quantitative analysis of optic disc cupping in compressive optic neuropathy. *Ophthalmology* 1995; **102**: 436–440.
5 Hayreh SS. Blood supply of the optic nerve head and its role in optic atrophy, glaucoma and oedema of the optic disc. *Br J Ophthalmol* 1969; **53**: 721–748.
6 Quigley HA, Green WR. The histology of human glaucoma cupping and nerve damage: clinicopathologic correlation in 21 eyes. *Ophthalmology* 1979; **10**: 1803–1827.
7 Roh S, Noecker RJ, Schuman JS, Hedges III TR, Weiter JJ, Mattox C. Effect of optic nerve head drusen on nerve fiber layer thickness. *Ophthalmology* 1998; **105**: 878–885.
8 Vizzeri G, Balasubramanian M, Bowd C, Weinreb RN, Medeiros FA, Zangwill LM. Spectral domain-optical coherence tomography to detect localized retinal nerve fiber layer defects in glaucomatous eyes. *Opt Express* 2009; **17**: 4004–4018.
9 Steel DH, Waldock A. Measurement of the retinal nerve fiber layer with scanning laser polarimetry in patients with previous demyelinating optic neuritis. *J Neurol Neurosurg Psychiatry* 1998; **64**: 505–509.
10 Reus NJ, Lemij HG. Relationship between standard automatic perimetry and GDx VCC measurements. *Inv Ophthalmol Vis Sci* 2004; **45**: 840–845.
11 Sanders EA, Volkers AC, Van der Poel JC, Van Lith GHM. Spatial contrast sensitivity function in optic neuritis. *Neuro-Ophthalmol* 1984; **4**: 255–259.
12 Optic Neuritis Study Group. The clinical profile of acute optic neuritis: experience of the optic neuritis treatment trial. *Arch Ophthalmol* 1991; **109**: 1673–1678.
13 Rosen JA. Pseudoisochromatic visual testing in the diagnosis of disseminated sclerosis. *Trans Am Neurol Assoc* 1965; **90**: 283–284.
14 Marré M. The investigation of acquired color deficiencies. In: *Second Congress of the International Color Association*, University of York, 2–6 July 1973; Adam Hilger Publishers: London, 1973.

15 Köllner H. *Die Störungen des Farbensinnes ihre klinische Bedeutung und ihre Diagnose*. Karger: Berlin, 1912.
16 Schneck ME, Haegerstrom-Portnoy G. Color vision defect type and spatial vision in the optic neuritis treatment trial. *Inv Ophthalmol Vis Sci* 1997; **38**: 2278–2289.
17 Pokorny J, Smith VC. Eye disease and color defects. *Vision Res* 1986; **26**: 1573–1584.
18 Poinoosawmy D, Nagasubramanian S, Gloster J. Color vision in patients with chronic simple glaucoma and ocular hypertension. *Br J Ophthalmol* 1980; **64**: 852–857.
19 Dacey DM, Peterson BB, Robinson FR, Gamlin PD. Fireworks in the primate retina: *in vitro* photodynamics reveals diverse LGN-projecting ganglion cell types. *Neuron Neurotechnique* 2003; **37**: 15–27.
20 Holopigian K, Seiple W, Mayron C, Koty R, Lorenzo M. Electrophysiological and psychophysical flicker sensitivity in patients with primary open-angle glaucoma and ocular hypertension. *Inv Ophthalmol Vis Sci* 1990; **31**: 1863–1868.
21 Vaegan, Graham SL, Goldberg I, Buckland L, Hollows FC. Flash and pattern electroretinogram changes with optic atrophy and glaucoma. *Exp Eye Res* 1995; **60**: 697–706.
22 Holopigian K, Greenstein VC, Seiple W, Hood DC, Ritch R. Electrophysiologic assessment of photoreceptor function in patients with primary open-angle glaucoma. *J Glaucoma* 2000; **9**: 163–168.
23 Fortune B, Bearse Jr MA, Cioffi GA, Johnson CA. Selective loss of an oscillatory component from temporal retinal multifocal ERG responses in glaucoma. *Inv Ophthalmol Vis Sci* 2002; **43**: 2638–2647.
24 Nork TM, Ver Hoeve JN, Poulsen GL, Nickells RW, Davis MD, Weber AJ *et al*. Swelling and loss of photoreceptors in chronic human and experimental glaucomas. *Arch Ophthalmology* 2000; **118**: 235–245.
25 Panda S, Jonas JB. Decreased photoreceptor count in human eyes with secondary angle-closure glaucoma. *Inv Ophthalmol Vis Sci* 1992; **33**: 2532–2536.
26 Kendell KR, Quigley HA, Kerrigan LA, Pease ME, Quigley EN. Primary open-angle glaucoma is not associated with photoreceptor loss. *Inv Ophthalmol Vis Sci* 1995; **36**: 200–205.
27 Wygnanski T, Desatnik H, Quigley HA, Glovinsky Y. Comparison of ganglion cell loss and cone loss in experimental glaucoma. *Am J Ophthalmol* 1995; **120**: 184–189.
28 Choi SS, Zawadzki RJ, Keltner JL, Werner JS. Changes in cellular structures revealed by ultra-high resolution retinal imaging in optic neuropathies. *Inv Ophthalmol Vis Sci* 2008; **49**: 2103–2119.
29 Choi SS, Zawadzki RJ, Greiner MA, Werner JS, Keltner JL. Fourier-domain optical coherence tomography and adaptive optics reveal nerve fiber layer loss and photoreceptor changes in a patient with optic nerve drusen. *J Neuro-Ophthalmol* 2008; **28**: 120–125.
30 Choi SS, Zawadzki RJ, Lim MC, Brandt JD, Keltner JL, Doble N *et al*. Evidence of outer retinal changes in glaucoma patients as revealed by ultrahigh resolution *in vivo* retinal imaging. *Br J Ophthalmol* 2011; **95**: 131–141.
31 Zawadzki RJ, Fuller AR, Wiley DF, Hamann B, Choi SS, Werner JS. Adaptation of a support vector machine algorithm for segmentation of retinal structures in volumetric optical coherence tomography data sets. *J Biomed Opt* 2007; **12**: 041206-1–041206-8.
32 Kim DY, Werner JS, Zawadzki RJ. Comparison of phase-shifting techniques for *in vivo* full-range, high-speed Fourier-domain optical coherence tomography. *J Biomed Opt* 2010; **15**: 056011-1–056011-8.
33 Choi SS, Doble N, Hardy JL, Jones SM, Keltner JL, Olivier SS *et al*. *In vivo* imaging of the photoreceptor mosaic in retinal dystrophies and correlations with visual function. *Inv Ophthalmol Vis Sci* 2006; **47**: 2080–2092.
34 Xue B, Choi SS, Doble N, Werner JS. Photoreceptor counting and image montaging of *en-face* retinal images from an adaptive optics fundus camera. *J Opt Soc Am* 2007; **24**: 1364–1372.
35 Zawadzki RJ, Jones SM, Olivier SS, Zhao M, Bower BA, Izatt JA *et al*. Adaptive-optics optical coherence tomography for high-resolution and high-speed 3D retinal *in vivo* imaging. *Opt Express* 2005; **13**: 8532–8546.
36 Miller DT, Kocaoglu O, Wang Q, Lee S. Adaptive optics and the eye (super resolution OCT). *Eye* (in press).
37 Zawadzki RJ, Cense B, Zhang Y, Choi SS, Miller DT, Werner JS. Ultrahigh-resolution optical coherence tomography with monochromatic and chromatic aberration correction. *Opt Express* 2008; **16**: 8126–8143.
38 Quigley HA, Addicks EM, Green WR. Optic nerve damage in human glaucoma. III. Quantitative correlation of nerve fiber loss and visual field defect in glaucoma, ischemic neuropathy, papilledema, and toxic neuropathy. *Arch Ophthalmol* 1982; **100**: 135–146.
39 Hood DC, Kardon RH. A framework for comparing structural and functional measures of glaucomatous damage. *Prog Ret Eye Res* 2007; **26**: 688–710.
40 Li KY, Roorda A. Automated identification of cone photoreceptors in adaptive optics retinal images. *J Opt Soc Am A* 2007; **24**: 1358–1363.
41 Curcio CA, Sloan KR, Kalina RE, Hendrickson AE. Human photoreceptor topography. *J Comp Neurol* 1990; **292**: 497–523.
42 Roorda A, Williams DR. Optical fiber properties of individual human cones. *J Vision* 2002; **2**: 404–412.
43 Guo L, Normando EM, Nizari S, Lara D, Cordeiro MF. Tracking longitudinal retinal changes in experimental ocular hypertension using the cSLO and spectral domain-OCT. *Inv Ophthalmol Vis Sci* 2010; **51**: 6504–6513.